WIND ENERGY

Wind Energ. 2010; **00**:1–26

DOI: 10.1002/we

RESEARCH ARTICLE

A Refined Tip Correction based on Decambering

Jens N. Sørensen, Kaya O. Dag and Néstor Ramos-García

DTU Wind Energy, Technical University of Denmark, 2800 Kongens Lyngby, Denmark

ABSTRACT

A new tip correction for use in performance codes based on the Blade Element Momentum (BEM) or the lifting line technique is presented. The correction modifies the circulation by taking into account the additional influence of the induction of the vortices in the wake, using the so-called decambering effect and thin-airfoil theory. A limitation of the standard Prandtl tip correction is that it represents the surface loading by a line distribution which does not take into account the actual shape of the rotor blade. Thus, the chord distribution does not appear as a parameter in the model, and the loading in the proximity of the tip is generally found to be overestimated. The new tip correction is implemented as an additional correction in order to represent the surface loading by a line distribution. Comparing computations using the new model with standard BEM results and computations using a 3D panel code show that the inclusion of the correction greatly improves the results. The new model also explains some of the discrepancies that earlier on have been observed when using a BEM technique based alone upon standard tip corrections.

KEYWORDS

Decambering; tip correction; wind turbine aerodynamics; wind turbine performance

Correspondence

Jens N. Sørensen, DTU Wind Energy, Technical University of Denmark, Nils Koppels Alle, Bldg. 403, 2800 Kongens Lyngby, Denmark.

E-mail: jnso@dtu.dk

Received . . .

Prepared using weauth.cls [Version: 2010/06/17 v1.00]

1. INTRODUCTION

The tip correction was originally introduced by Prandtl in an appendix to the dissertation of Betz (1919) as a means to correct the loading obtained from axisymmetric momentum theory to account for the difference between a rotor with infinitely many blades and a realistic rotor with a finite number of blades. The correction illustrated the ingenious way Prandtl introduced simple engineering solutions to complicated problems. Betz formulated the concept of the optimum rotor with a finite number of blades, by stating that maximum efficiency is obtained when the pitch of the trailing vortices in the wake of the rotor is constant and each trailing vortex sheet translates backward as an un-deformed regular helicoidal surface with a constant speed. This was essentially inspired from the lifting line theory for a planar wing, which states that maximum efficiency is obtained when a constant downwash is produced. However, at that time it was not possible to actually solve the problem, although Goldstein (1929) some years later showed that a solution indeed could be obtained using infinite series of Bessel functions. The way Prandtl solved the problem was to approximate the helical wake with a series of planar vortex surfaces and determine the tip correction as the ratio between the circulation of an N-bladed rotor and the circulation of a rotor with infinitely many blades. For the latter, the circulation was determined as the jump in velocity potential over the vortex sheet (see Tollmien et al., 1961). The outcome of this analysis was a simple expression giving the load reduction as a function of tip speed ratio, flow angle and distance from the tip of the rotor. This correction was later slightly modified by Glauert (1935), who combined it with the Blade-Element-Momentum (BEM) theory, as a simple remedy to take into account the difference between the blade element approach and the axisymmetric momentum theory. Although the theory today is routinely used as a tool for designing and analyzing wind turbine rotors, it is also criticized for not representing accurately the loading in near vicinity of the tip of the rotor. This has led to different versions of the original formulation (e.g. de Vries, 1979) and in a recent work of Shen et al. (2005) it was shown that the original formulation contains an inconsistency which, to a certain extent, can be remedied by introducing a further correction. Another problem with the tip correction is that it does not take into account the actual shape of the rotor blade. Thus, the chord distribution does not appear as a parameter in the model and it seems that something more than just accounting for the number of finite blades is missing in the expression. This is further demonstrated with the development of the actuator line technique. The actuator line technique was developed by Sørensen and Shen (2002) as a means of introducing a lifting line model into the Navier-Stokes equations. In the model, the loading, which is obtained from tabulated airfoil data, is distributed along lines representing the rotor blades. Using this approach it should in principle not be necessary to introduce any tip correction, since the loading is obtained directly on each individual blade. Nevertheless, the loading in the proximity of the tip seems always to be overestimated, suggesting that some additional correction is

Wind Energ. 2010; **00**:1–26 © 2010 John Wiley & Sons, Ltd.
DOI: 10.1002/we
Prepared using weauth.cls

required in order to represent the surface loading by a line distribution.

In a short report, published in conjunction with a plenary meeting within a European project, Montgomerie (1995) demonstrated that an error is introduced when using the lifting line or the BEM method in their usual form. This error is caused by the fact that these methods rely on the blade representation being a line instead of a surface. Indeed, the downwash induced by the vortex system in the wake causes a curved streamline along the chord line that virtually corresponds to an additional negative camber of the airfoil. Since the induction generally will be higher at the trailing edge, which is the line from which the trailing vortices are shed into the wake, than at the leading edge, the aerodynamic consequence is that the effect of the induction from the free vortices is felt as a decambering of the airfoil. Hence it tends to increase the zero lift angle and by this decrease the loading. The effect is, just as for the usual tip correction, felt everywhere on the blade, but most significantly close to the tip. To illustrate the decambering effect, Fig. 1 shows how the local induction affects the aerodynamic characteristics of the local airfoil section. It is here seen how the downwash from the free vortices induce a local velocity field that changes along the chord line.

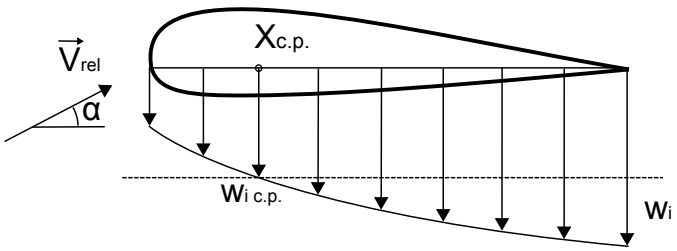

Figure 1. Downwash due to the induction of the free vortices in the wake

In a lifting line technique, only the velocity component at the c/4 position is used to compute the relative velocity and angle of attack. However, as can be seen from the figure, there is an additional velocity component, $\Delta w_i = w_i - w_{c.p.}$, that is positive from the leading edge to the center of pressure, $x_{c.p.}$, and negative from the center of pressure to the trailing edge. Thus, as seen from the airfoil, the additional velocity is felt as curved streamlines, which consequently represents a negative bending of the airfoil. This is shown in Figs. 2(a) and 2(b), which illustrates how the induced velocity of the free vortex wake is felt as a negative bending of the chord line. This effect was discussed by Montgomerie (1995) and referred to as decambering. It should be noted, that decambering also has been employed to correct airfoil data for curvature effects in aerodynamic models of vertical axis turbines (see Migliore et al., 1980; Bianchini et al., 2011). Furthermore, the term

DOI: 10.1002/we

is also employed for post-stall predictions using lifting line or vortex-lattice models (see Mukherjee and Gopalarathnam, 2006).

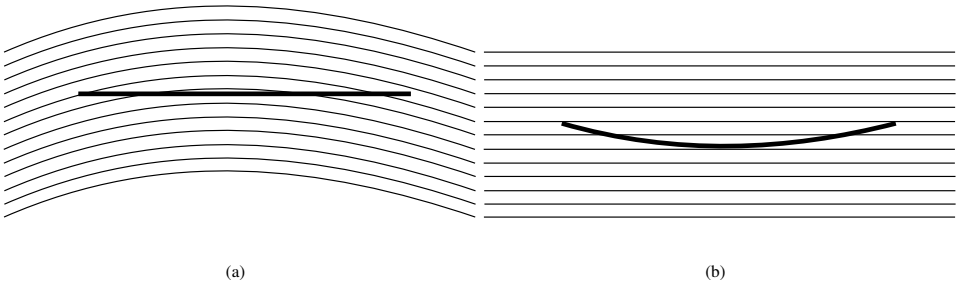

Figure 2. (a) Curved streamlines representing the additional downwash from the induction of the free vortices in the wake. (b) The effect from the additional downwash seen as an effective negative bending (decambering) of the airfoil.

In this paper, a technique based on the Biot-Savart induction law is introduced, which can be used to determine the effect of decambering. Furthermore, using thin airfoil theory, a simple correction technique is developed by which the loading from lifting line or BEM models can take into account the decambering effect and employ it together with the usual tip correction. By comparing the results from the model with a more advanced numerical technique representing the surface of the rotor, it will be shown that the introduction of a decambering correction indeed explains most of the discrepancies attained when using the lifting line technique or a BEM model with only a Prandtl tip correction.

The paper is organized as follows. In section 2, the equations and the technique behind the decambering tip correction are introduced. In section 3, the lifting line, the BEM method, and their coupling with the new tip correction are described. Furthermore, the vortex-lattice (panel) method used to validate the correction is described. In section 4, the new technique is validated against the vortex-lattice method. Finally, the work is concluded in section 5.

2. THE DECAMBERING CORRECTION

Figs. 3(a) and 3(b) show a translating and a rotating wing, and the associated distribution of circulation of a simplified vortex system consisting of trailing vortex lines. Along the center of pressure, which here is taken as the c/4-chord line of the wing, is shown the bound vorticity. The lines extending downwards from the bound vortex line constitutes the trailing vortices. The strength of the trailing vortices is determined from the distribution of the circulation of the bound vortex. Representing the bound circulation distribution by discrete values Γ_i, with $i = 1,2, ..., N$, where $i = 1$ represents the root

Wind Energ. 2010; **00**:1–26
DOI: 10.1002/we

and $i = N$ the tip, the associated system of trailing vortices are given as horseshoe vortices with strength $\hat{\Gamma}_i = \Gamma_{i+1} - \Gamma_i$. In the case of a planar wing, the trailing vortices are straight lines, whereas they form a helical spiral with a helical pitch corresponding to the local flow angle in the case of a rotor blade. It is the effect from the trailing vortices that induces a downwash along the chord line which, for each cross section, causes the decambering effect. The resulting correction is carried out in a series of control points, which in the spanwise direction are located at the midpoint of each bound vortex filament.

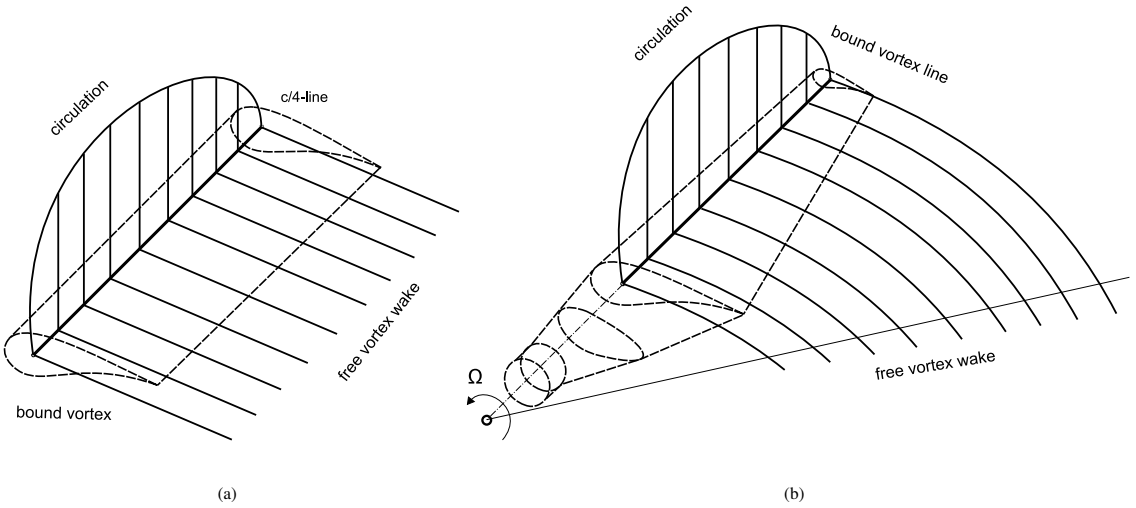

Figure 3. (a) Translating wing and associated vortex lines. (b) Rotating wing and associated vortex lines.

The induction is determined from the Biot-Savart induction law according to the following compact formula (see Katz and Plotkin, 2001):

$$\vec{q} = \frac{\Gamma}{4\pi} \frac{(r_1 + r_2)(\vec{r_1} \times \vec{r_2})}{r_1 r_2 (r_1 r_2 + \vec{r_1} \cdot \vec{r_2})}, \tag{1}$$

where $\vec{r}_1$ and $\vec{r}_2$ denote the position vectors between the control point and the two edges of the discretized vortex filament. In order to determine the effect of the downwash on the airfoil characteristics, thin-airfoil theory is employed. This is accomplished by dividing each airfoil section into a set of evaluation points following a cosine distribution. This distribution is sketched in Fig. 4(a), from which it can be seen that the evaluation point, x_k, is given as

$$x_k = \frac{c}{2}(1 - cos\theta_k), \tag{2}$$

where

$$\theta_k = \pi \frac{k-1}{M-1}, \quad k \in [1, M]. \tag{3}$$

DOI: 10.1002/we

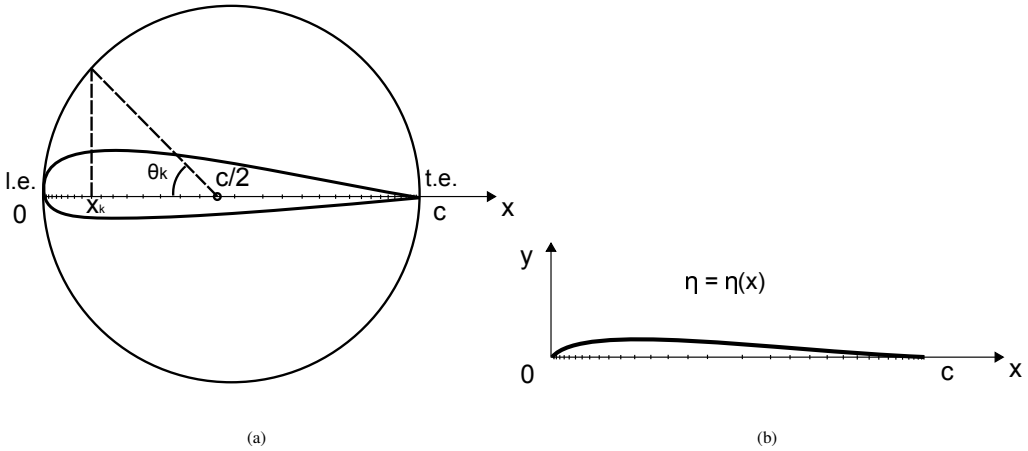

(a) (b)

Figure 4. (a) Distribution of evaluation point, x_i, along the chord line. (b) Representation of the camber line $\eta = \eta(x)$.

Here M denotes the number of evaluation points. The evaluation points are located along the chord line with the leading edge at $x = 0$ $(\theta = 0)$ and the trailing edge at $x = c$ $(\theta = \pi)$. The camber line of an airfoil is usually a known function, $\eta_c = \eta_c(x)$ (see Fig.4(b)). However, in the present case the camber line is formed from the additional induction of the free vortices along the chord line. From thin-airfoil theory, it is known that the slope of the local (total) velocity is equal to the camber line slope. Hence,

$$\frac{d\eta_c}{dx} = \frac{w}{u}, \tag{4}$$

where (u, w) denotes the velocity components tangential and normal to the chord lines, respectively. For each evaluation point on the chord line, the induced velocity is determined as the sum of contributions from the vortex segments of each of the N trailing vortices. Thus, for a wing section subject to a local relative velocity, $\vec{V}_{rel}$, and angle of attack, α_j, the induced velocity can be written as

$$w_{jk} = \sum_{i=1}^{N} a_{ijk}\Gamma_i, \quad u_{jk} = \sum_{i=1}^{N} b_{ijk}\Gamma_i \tag{5}$$

Where a_{ijk} refers to the induced normal velocity on evaluation point k on chord line j due to the induction from vortex i with unit strength, and w_{jk} is the corresponding induced velocity, resulting from the induction of all free vortices, each of strength Γ_i. Likewise, b_{ijk} refers to the induced velocity in the tangent direction to the chord line. For simplicity, assuming that the center of pressure is located at the c/4 point, the additional camber line slope is determined by subtracting the local induction by the induction at the c/4-point. Thus, at each control point the additional slope due to the decambering effect reads

$$\left.\frac{d\eta_c}{dx}\right|_{jk} = -\frac{w_{jk} - w_{j,c/4}}{||V_{rel,j}|| \cos\alpha_j + u_{jk} - u_{j,c/4}}, \tag{6}$$

Wind Energ. 2010; **00**:1–26

DOI: 10.1002/we

where $w_{j,c/4} = \sum_{i=1}^{N} a_{ij,c/4}\Gamma_i$ and $u_{j,c/4} = \sum_{i=1}^{N} b_{ij,c/4}\Gamma_i$, with $a_{ij,c/4}$ referring to the induced normal velocity on the c/4-chord line j due to the interaction from unit vortex i and $b_{ij,c/4}$ the same for the tangential velocity. Note that the minus sign in eq.6 is introduced because the decambering denotes the effect of the additional streamline curvature seen from the airfoil.

For an airfoil with camber and zero-lift angle α_{L0}, the lift coefficient is given as

$$C_l = 2\pi(\alpha - \alpha_{L0}) \tag{7}$$

Thus, the difference in lift coefficient between an airfoil with and without camber is given as

$$\Delta C_l = -2\pi\alpha_{L0} \tag{8}$$

According to Katz and Plotkin (2001), the zero-lift angle can be determined from the following expression:

$$\alpha_{L0} = -\frac{1}{\pi}\int_0^{\pi} \frac{d\eta_c}{dx}(\cos\theta - 1)d\theta. \tag{9}$$

Combining eqs. 6 and 9 yields

$$\alpha_{L0} = \frac{1}{\pi}\int_0^{\pi} \left(\frac{w_{jk} - w_{j,c/4}}{||V_{rel,j}||\cos\alpha_j + u_{jk} - u_{j,c/4}}\right)(\cos\theta - 1)d\theta. \tag{10}$$

Replacing the integration with a discrete summation, the following formula is obtained for correcting the lift coefficient at cross section j:

$$\Delta C_{l,j} = -2\Delta\theta \sum_{k=1}^{M} \frac{(w_{jk} - w_{j,c/4})(\cos\theta_k - 1)}{||V_{rel,j}||\cos\alpha_j + (u_{jk} - u_{j,c/4})}, \tag{11}$$

where $\Delta\theta = \pi/(M-1)$. In order to correct directly on the circulation distribution, the Kutta-Joukowsky theorem is employed,

$$\Gamma = \frac{1}{2}cV_{rel}C_l. \tag{12}$$

Combining eqs. 11 and 12, assuming that $(u_{jk} - u_{j,c/4}) << V_{rel,j}$, results in the following correction formula

$$\Delta\Gamma_j = \frac{\Delta\theta \cdot c_j}{\cos\alpha_j}\sum_{k=1}^{M}(w_{jk} - w_{j,c/4})(\cos\theta_k - 1). \tag{13}$$

Eqs. 5 and 13 form the final set of equations for correcting the circulation due to the decambering effect of the free wake vortices. It is easily seen that the system constitutes an implicit set of equations, since the induced velocity depends on the circulation that is being corrected. The system may either be solved iteratively or as a full matrix system. In the latter case,

DOI: 10.1002/we

combining eqs. 5, 8, 12 and 13, the full system may be written as

$$\Gamma_j + \frac{\Delta\theta c_j}{\cos\alpha_j}\sum_{k=1}^{M}\sum_{i=1}^{N}(a_{ijk} - a_{ij,c/4})(\cos\theta_k - 1)\Gamma_i = \frac{1}{2}c_j V_{rel,j}\bar{C}_{l,j}, \tag{14}$$

where $\bar{C}_{l,j}$ is the lift coefficient obtained directly from the relative velocity, i.e. without the decambering correction. Eq. 14 can be written in a more compact form as follows,

$$\sum_{i=1}^{N} d_{ij}\Gamma_i = e_j, \quad j = 1, 2, ..., N, \tag{15}$$

where

$$d_{ij} = \delta_{ij} + \frac{\Delta\theta c_j}{\cos\alpha_j}\sum_{k=1}^{M}(a_{ijk} - a_{ij,c/4})(\cos\theta_k - 1) \quad \text{and} \quad e_j = \frac{1}{2}c_j V_{rel,j}\bar{C}_{l,j}, \tag{16}$$

with δ_{ij} denoting the Kronecker delta. In the expression, the coefficient a_{ijk} depends on the geometry of the wing and on the local flow angles at which the free vortices are shed into the wake. Thus, for a given wing geometry, d_{ij} may once and for all be computed for various flow angles and subsequently be determined by interpolation in the performance computations. To be in accordance with thin-airfoil theory, the center of pressure was assumed to be located in the c/4-point. However, for a typical wind turbine airfoil this is normally located close to the c/3-point. Nevertheless, this depends on the spanwise location and operating conditions. To evaluate the error committed by having an offset between the actual center of pressure and the one employed in the analysis, a simple estimate can be made by assuming a linear distribution of additional induction. The equation forming the background from this analysis is derived in **Appendix A**. From this we get that utilizing the c/4-point instead of the c/3-point results in a change in the correction of the angle of attack of 16%. As an example, a correction $\Delta\alpha = 6^\circ$ would be reduced to $\Delta\alpha = 5^\circ$. In the next section, the application of the correction together with the lifting line technique and the BEM method will be presented.

3. AERODYNAMIC MODELING

In this section, different aerodynamic models are introduced. In particular, the lifting line method and the Blade-Element Momentum (BEM) techniques, which both will be used together with the new decambering technique, are presented. To validate the technique, a 3D panel method is employed, which will also be explained.

3.1. Lifting line method

In the lifting line method, the vorticity on the wing and in the wake are represented by horseshoe vortices in a way similar to the sketches shown in Figs. 3(a) and 3(b). The induction from the trailing vortices is computed from Eq. 1 and the local

DOI: 10.1002/we

relative velocity is subsequently calculated at the c/4-point and employed to compute the local angle of attack. The resulting lift coefficient distribution is then determined from tabulated airfoil data. In order to determine the strength of the trailing vortices, the Kutta-Joukowsky theorem, Eq. 12, is employed, which subsequently is corrected for the influence of decamber by solving eqs. 14 - 16. It is clearly seen that this technique is very well suited to include the influence of decamber as we are employing the same vortex system for computing the angle of attack as for computing the downwash forming the input to the decambering correction. In the present implementation, the overall numerical technique for determining the circulation distribution is iterative, and the vortices in the wake are prescribed to be located in the plane of the wing.

3.2. The Blade-Element Momentum (BEM) method

The BEM method was developed by Glauert (1935) as a practical way to analyse and design rotor blades. In the BEM method the interference factors, a and a', are introduced as follows

$$a = 1 - u_R/U_0 \quad \text{and} \quad a' = \frac{u_\theta}{2\Omega r}, \tag{17}$$

where u_R is the axial velocity in the rotor plane, U_0 is the wind speed, u_θ is the rotational velocity in the wake just after the rotor, and Ωr is the local tangential velocity of the rotor at position r. The loading is computed by combining a local blade element using tabulated 2-dimensional airfoil data and the 1-dimensional momentum theory. Carrying out the analysis (see e.g. Hansen, 2008), the following relations are obtained

$$a = \frac{1}{4Fsin^2\phi/(\sigma C_l cos\phi) + 1}, \tag{18}$$

and

$$a' = \frac{1}{4F\cos\phi/(\sigma C_l) - 1}, \tag{19}$$

where $\sigma = N_b c/2\pi r$ is the solidity, with N_b denoting the number of blades. ϕ is the local flow angle, $\tan\phi = \frac{U_0(1-a)}{\Omega r(1+a')}$, and F is the Prandtl 'tip correction' factor to account for a finite number of blades,

$$F = \frac{2}{\pi}\cos^{-1}\left[exp(-\frac{N_b(R-r)}{2rsin\phi})\right], \tag{20}$$

where R is the radius of the rotor. Eqs. 18 - 20 are solved iteratively at each cross section, using tabulated airfoil data to determine the local flow properties. After each iteration, the decambering correction is introduced by correcting the circulation by solving eqs. 14 - 16. The induction coefficients in Eq. 5 are determined by computing the induction from the trailing vortices in the wake. These are represented by a number of helical segments, which are released from the trailing edge with the local flow angle, ϕ, and followed a certain distance downstream in the wake. Note that the decambering

DOI: 10.1002/we

correction, Eq. 15, forms a $N \times N$ system whereas the BEM method is a $2 \times N$ system, meaning that the inclusion of the decambering correction is more computational costly that the BEM in itself. There is certainly room for making the technique more computationally efficient. This, however, is not the scope of the present work, where the main aim is to illustrate that the correction is required in order to obtain reliable results when using the BEM method.

3.3. The vortex lattice (panel) method

This method is introduced in order to validate the developed correction. In the panel method the surface of the lifting body is simulated by a distribution of quadrilateral singularities satisfying the no-penetration velocity condition. In the present work, both the inviscid and the viscous version of the in-house developed MIRAS code (Ramos-García et al., 2013) are employed. In the inviscid part of the model, the problem is considered in two regions: the surface, which is represented by quadrilateral sources and dipoles, and the wake, which is modeled by vortex filaments. The vortex wake is released at the trailing edges using the unsteady Kutta-Joukowsky condition of zero trailing edge loading. To satisfy this condition, at each time step a quadrilateral panel with a doublet distribution is created as the first wake panel for each one of the span-wise stations. The strength of these panels is equal to the difference between the corresponding upper and lower trailing edge quadrilateral doublets. The filaments are subsequently convected downstream according to the induction law of Biot-Savart, introducing a viscous core model to approximate viscous diffusion and thus including vortex core growth and vortex straining. More details about the model, including a thorough validation, can be found in Ramos-García et al. (2014).

4. RESULTS AND DISCUSSION

In this section, the new tip correction is validated against results obtained from the MIRAS code. The computations are carried out both for planar translating wings and wind turbine rotor configurations.

4.1. Planar translating wing

In what follows, the results from the lifting line method described in section 3.1 are compared with the MIRAS panel code. For comparison, the computations are carried out both with and without the new tip correction. The examples considered are planar wings with constant chord consisting of NACA 0012 or 4412 airfoil sections, and at different aspect ratios. From 2D viscous-inviscid computations, employing a 2D version of the MIRAS code, the lift coefficient for 2D airfoil sections has been calculated and approximated as $C_l \simeq 0.12 \cdot \alpha^\circ$ for the NACA 0012 airfoil and as $C_l \simeq 0.12 \cdot \alpha^\circ + 0.5$ for the

Wind Energ. 2010; **00**:1–26
DOI: 10.1002/we

NACA 4412 airfoil. These expressions are those used in Eq. 12 to obtain the circulation distribution. In Figs. 5(a)-5(f), computed circulation distributions for six different wing configurations are compared. The lifting line computations are labeled $'LLT'$ and the corresponding results applying the decambering correction are labeled $'decam-LLT'$. In the figures, the circulation is made dimensionless by $2\pi cU_0$, where c is the chord length and U_0 is the free-stream velocity. As the circulation distribution is symmetric, only one half of the distribution is presented for each case. It is clearly seen that the inclusion of the decambering effect improves the results. Generally, the lifting line technique is over-predicting the circulation with 10-15%, whereas the inclusion of the decambering correction ensures a circulation distribution that within plotting accuracy corresponds to what is obtained when using a full panel discretization of the surface. From the figure is seen that the decambering correction works for both symmetric and unsymmetrical airfoils and for all aspect ratios considered.

4.2. Rotating wing

To validate the effect of using the decambering correction on a rotating wing, the correction is employed together with the BEM method. In this method, it is still necessary to use the Prandtl tip correction to correct for finite number of blades in the momentum theory. Hence, it is required to apply both the Prandtl tip correction and the decambering correction.

4.2.1. Simple optimally designed rotors

In this part of the study, the influence of different number of blades is analyzed. For this purpose three wind turbine rotors equipped with one, two or three blades are designed using the technique for designing aerodynamically optimum planforms outlined in Burton et al. (2002). In this technique, it is assumed that the optimum interference factors take the values

$$a_{opt} = 1/3 \quad \text{and} \quad a'_{opt} = \frac{2}{9\lambda^2 y^2}, \tag{21}$$

where $y = r/R$ and λ is the tip speed ratio. The general expression to determine the planform is as follows:

$$N_b C_l \left(\frac{c}{R}\right) = \frac{8\pi \cos\phi a'}{1+a'} y, \tag{22}$$

with the corresponding twist angle distribution:

$$\beta = \tan^{-1}\left(\frac{1-a}{\lambda y(1+a')}\right). \tag{23}$$

It should be noted the Prandtl tip correction has not been included in the equations for the design of the rotor.

DOI: 10.1002/we

Prepared using weauth.cls

To simplify the geometry, the NACA 4412 airfoil is used along the entire span and the rotor is optimized to operate at a tip speed ratio, $\lambda = 6$, and an optimum angle of attack of 1.7°, corresponding to $C_l = 0.7$. To simplify further, the expression for the chord distribution, Eq. 22, is replaced by a linear expression with the same slope as at the $y = 80\%$ point. For a three-bladed rotor, this results in a blade with a chord length ranging linearly from 0.156R at the root to 0.06R at the tip. From Eq. 22, it is readily seen that rotors with other blade numbers are designed simply by scaling the chord distribution by the number of blades, and Eq. 23 shows that the twist distribution is invariant to the number of blades. The chord distribution for a three-bladed rotor designed from this technique is shown in Fig.6 and the associated twist distribution is plotted in Fig.7.

In Figs. 8(a)-8(d), 9(a)-9(d) and 10(a)-10(d) the computed circulation distributions are shown for one-bladed, two-bladed and three-bladed rotors respectively. In the figures, the circulation is made dimensionless by RU_0, where R is the rotor radius and U_0 is the free-stream velocity. The plots compare BEM results, both with and without the decambering correction, with results from the MIRAS panel code at different tip speed ratios. In all the depicted cases, it is clear that the decambering correction has a positive effect on the resulting circulation distribution. In most cases the improvement in the circulation is in of the order of 10-15%, being most significant, however, for the one-bladed rotor. As can also be seen from the figures, the computations without the decambering correction always over-predict the circulation. Hence, the word decambering should be taken literally in the sense that the effective lift distribution, and by this the circulation, is always being reduced when using the correction.

Wake dependency

To use the method in combination with the BEM technique, a helical wake sheet is generated by using the local axial induction values from BEM calculation to define the helical pitch. The length of each vortex line is taken to be three rotations for the correction. However to analyze the dependency of the wake length, simulations are conducted with different wake lengths. For this purpose, the three-bladed optimally designed rotor with $\lambda = 9$ is used. As can be seen from Fig. 11 that a wake length corresponding to 30° of the rotation is enough for correcting the additional curvature effects from the wake. To be on the safe side, a wake length corresponding to a 90° rotation has been used.

4.2.2. The NREL 5 MW reference rotor

In order to validate further the decambering correction, simulations have been carried out for the NREL 5 MW virtual reference rotor. The NREL 5 MW reference wind turbine was designed by Jonkman et al. (2009) in order to have a

Wind Energ. 2010; **00**:1–26
DOI: 10.1002/we

common test case for comparing different aero-elastic tools. The turbine does not represent an actual wind turbine, but is designed as a good approximation of what an actual wind turbine of the associated size would be like. The diameter of the rotor is 128 m and the blade geometry is based on cylindrical cross sections on the inner part, DU21 - DU40 airfoils at the mid-part and on NACA 64 series airfoils on the outer part. A full description, including airfoil data, can be found in Jonkman et al. (2009).

In the following, a comparison between viscous MIRAS simulations and BEM with and without the decambering correction will be presented for the reference rotor. The viscous MIRAS simulations were performed on a surface mesh consisting of 20 spanwise cells and 160 chordwise cells, and 16 wake revolutions were simulated with an angular discretization of 10°. Viscous effects were taken into account in the potential panel code by employing the transpiration velocity concept and solving the integral boundary layer equations with free laminar to turbulent transition and a turbulent intensity of 0.1%. For further information on the 3D viscous-inviscid coupling technique, the reader is referred to Ramos-García et al. (2014). The airfoil polars used in the BEM calculations were obtained from 2D viscous-inviscid Q^3UIC computations for the local airfoil geometry at the different spanwise locations. More details on the viscous-inviscid interaction technique can be found in Ramos-García et al. (2013).

In Figs. 12(a)-12(f), comparisons between the calculated normal and tangential forces for the wind speeds of 6 m/s, 8 m/s and 10 m/s are displayed. For the tangential loading in the inner part of the blade, the BEM computations are in good agreement with the viscous MIRAS computations. However, in the outer part, the BEM computations overestimate the forces. In terms of the normal forces, BEM computations are consistently overpredicting the loading along the whole blade span.

Since the decambering correction is applied to the circulation and therefore only influencing the lift force, it has a minor effect on the tangential load at small angles of attack, showing that the power performance of the rotor is practically unchanged by the correction. Comparing the results for the normal load shows that the decambering correction alleviates the loading by 7-8% on the outer 10% of the blade. The normal load from the BEM computations, however, seems in all cases to be too high at the outer 30% of the blade, as compared to the MIRAS code.

DOI: 10.1002/we

4.2.3. The experimental MEXICO rotor

The MEXICO experiment is used as a final validation of the presented decambering correction. The MEXICO experimental campaign was carried out on a three-bladed wind turbine model of diameter 4.5 m. Measurements were performed under controlled conditions in the Large Scale Low Speed Facility of the German-Dutch Wind Tunnel Organization DNW in a 9.5 X 9.5 m^2 open test section. For the present analysis, two wind speed cases are taken into account, 15 m/s and 24 m/s. In both cases the rotor angular velocity is set to 424.5 rpm and the blades are subjected to a collective pitch of -2.3°. For more detailed information about the MEXICO experiment, the reader is referred to Schepers and Snel (2007).

MIRAS simulations were performed using a surface mesh consisting of 20 spanwise and 50 chordwise cells for each of the three blades. In terms of wake discretization, a 20° angular discretization was used with a total amount of 20 simulated wake revolutions in all cases. Laminar to turbulent transition was forced to take place at 5% of the chord from the leading edge on both the upper and lower sides of the airfoil sections throughout the blade span.

The calculated normal and tangential forces for the wind speeds of 15 m/s and 24 m/s are shown in Figs. 13(a)-13(d). There is an excellent agreement between measured data and MIRAS simulations. For all cases, it is observed how the decambering correction applied to the BEM calculations bring the predicted values closer to the measured data. For the tangential forces the decambering effect has a slightly stronger influence than for the NREL 5 MW case, increasing with the wind speed. The decambering correction influences the normal force exclusively in the near tip region, rounding up its peak distribution in a similar fashion as the MIRAS calculations. However, the normal load from the BEM computations seems in all cases to be too high at the outer 40% of the blade, as compared with experiments and the MIRAS simulations.

5. CONCLUSIONS

A refined tip correction based on thin airfoil theory and the induction from the vortices in the wake has been developed. The technique corrects the circulation obtained in lifting line or Blade-Element-Momentum (BEM) computations for the difference between a line load and a surface load using the so-called decambering approach. Decambering refers to the fact that the induction from the vortices in the wake by the airfoil is seen as an inverse cambering of the chord line. The resulting correction formula is derived by combining the Biot-Savart induction law with thin-airfoil theory. The developed correction has been implemented both in a lifting line model and in a BEM model as an additional correction to the Prandtl

Wind Energ. 2010; **00**:1–26 © 2010 John Wiley & Sons, Ltd.
DOI: 10.1002/we
Prepared using weauth.cls

tip correction. Comparisons to results from a 3D panel code show that the new correction greatly improves the circulation at the outer part of the rotor blade. The comparison comprises both planar translating wings as well as one-, two- and three-bladed rotors, including the NREL 5 MW reference rotor and the MEXICO model rotor. The correction is most significant for rotors with few blades, corresponding to rotor blades with low aspect ratios. For rotor blades with tapered tip geometries the correction mainly reduces the thrust at the outer part of the blade whereas the change in power performance is small. A main conclusion is that the inclusion of the decambering correction only changes slightly the predicted performance of the rotor, whereas it alleviates the loading by 7-8% at the outer part of the rotor blade.

ACKNOWLEDGEMENTS

The present work has been carried out with the support of the Danish Council for Strategic Research for the project Center for Computational Wind Turbine Aerodynamics and Atmospheric Turbulence (grant 2104-09-067216/DSF) (COMWIND). http://www.comwind.org

A. ERROR ESTIMATE FOR CENTER OF PRESSURE OFFSET

Assume a linear distribution of the additional induction as

$$\frac{\sum w}{V_{rel} cos\alpha} = a + (b-a)\left(\frac{x}{c}\right) \tag{A.1}$$

where a is the additional induction at the leading edge and $(b-a)$ is the slope. Then the local $\frac{d\eta}{dz}$ reads

$$\frac{d\eta}{dx} = \frac{\sum w - w_{c.p.}}{V_{rel}\cos\alpha} = (b-a)\left[\left(\frac{x}{c}\right) - \left(\frac{x}{c}\right)_{c.p.}\right]. \tag{A.2}$$

From thin airfoil theory, we have

$$\alpha_{L0} = -\frac{1}{\pi}(b-a)\int_0^\pi \left[\left(\frac{x}{c}\right) - \left(\frac{x}{c}\right)_{c.p.}\right](\cos\theta - 1)d\theta \tag{A.3}$$

and

$$\frac{x}{c} = \frac{1}{2}(1 - cos\theta). \tag{A.4}$$

By combining Eqs.A.3-A.4

$$\alpha_{L0} = -\frac{1}{\pi}(b-a)\int_0^\pi \left[\frac{1}{2}(1-cos\theta) - \frac{1}{2}(1-cos\theta_{c.p.})\right](\cos\theta - 1)d\theta \tag{A.5}$$

$$\begin{aligned}
\rightarrow \alpha_{L0} &= -\frac{1}{2\pi}(b-a)\int_0^\pi [cos\theta_{c.p.} - cos\theta](\cos\theta - 1)d\theta \\
\rightarrow \alpha_{L0} &= -\frac{1}{2\pi}(b-a)\int_0^\pi [(cos\theta_{c.p.} + 1)cos\theta - cos^2\theta - cos\theta_{c.p.}]d\theta \\
\rightarrow \alpha_{L0} &= \frac{1}{2\pi}(b-a)\left[\frac{\pi}{2} + \pi\cos\theta_{c.p.}\right] = \frac{1}{4}(b-a)[1 + 2\cos\theta_{c.p.}] \\
\rightarrow \alpha_{L0} &= \frac{1}{4}(b-a)\left[1 + 2 - 4\left(\frac{x}{c}\right)_{c.p.}\right] \\
\rightarrow \alpha_{L0} &= (b-a)\left[\frac{3}{4} - \left(\frac{x}{c}\right)_{c.p.}\right],
\end{aligned} \tag{A.6}$$

and the relative error becomes

$$\frac{\Delta\alpha_{L0}}{\alpha_{L0,c/4}} = \frac{\alpha_{L0} - \alpha_{L0,c/4}}{\alpha_{L0,c/4}} = \frac{\left[\frac{3}{4} - \left(\frac{x}{c}\right)_{c.p.} - \frac{1}{2}\right]}{\frac{1}{2}} = \frac{1}{2} - 2\left(\frac{x}{c}\right)_{c.p.} \tag{A.7}$$

Wind Energ. 2010; **00**:1–26

DOI: 10.1002/we

Prepared using weauth.cls

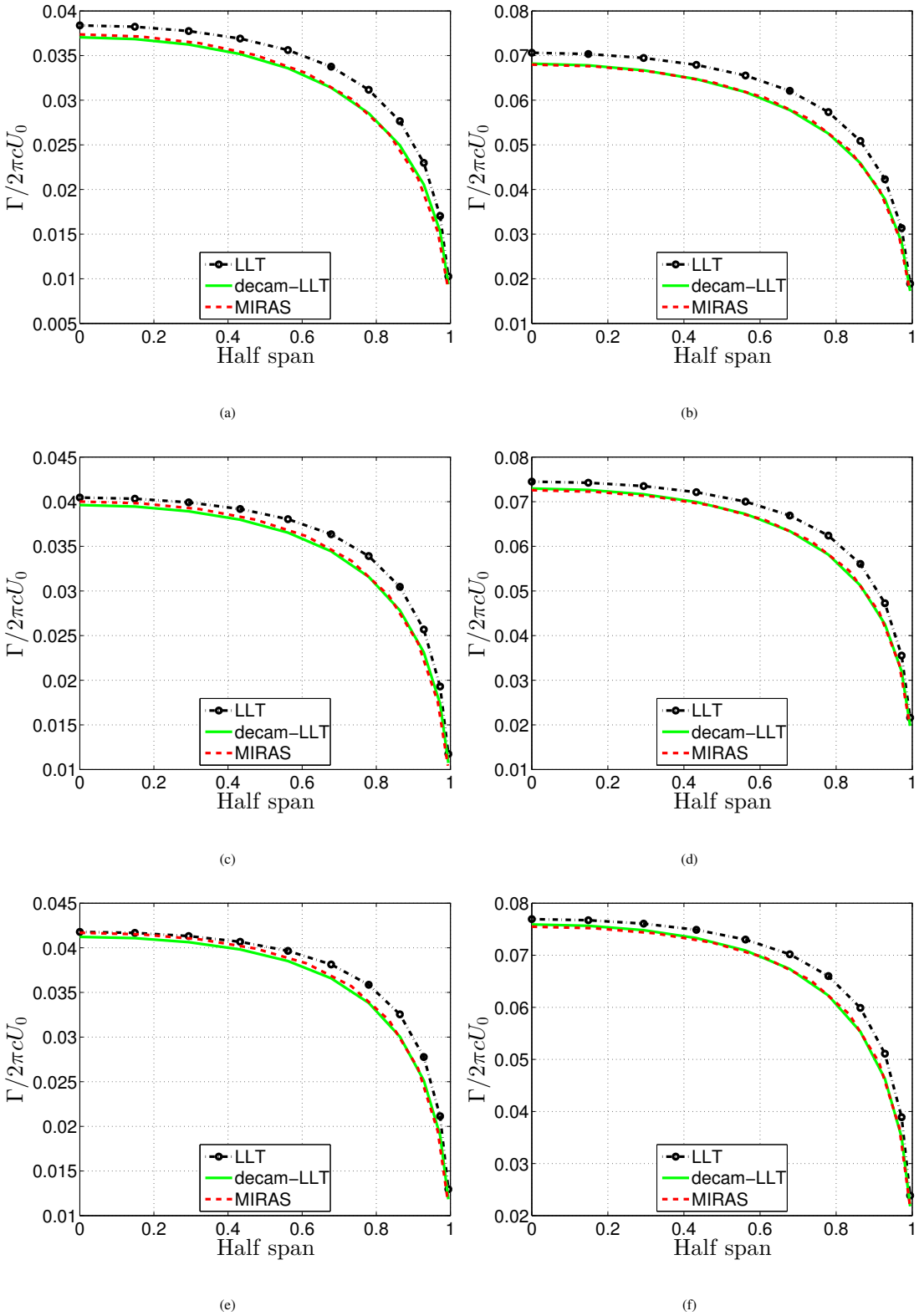

Figure 5. Distributions of normalized circulation, $\Gamma/2\pi cU_0$, for the planar wing configurations at a geometrical angle of attack of 5°.

a)NACA0012 AR=6, b)NACA4412 AR=6, c)NACA0012 AR=8,

d)NACA4412 AR=8, e)NACA0012 AR=10, f)NACA4412 AR=10

DOI: 10.1002/we

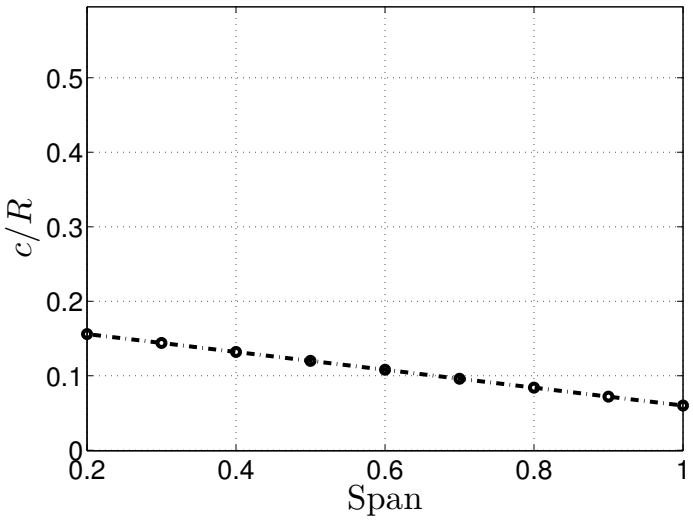

Figure 6. Chord distribution of the three bladed optimum rotor.

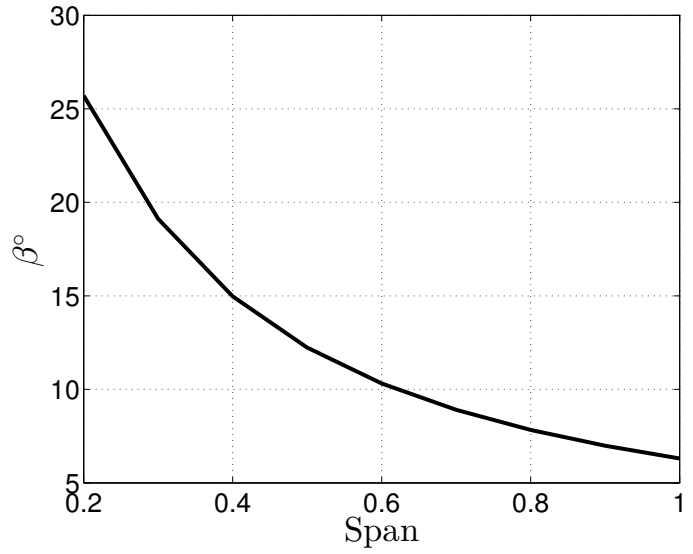

Figure 7. Twist distribution of the optimum rotors.

Wind Energ. 2010; **00**:1–26 © 2010 John Wiley & Sons, Ltd.

DOI: 10.1002/we

Prepared using weauth.cls

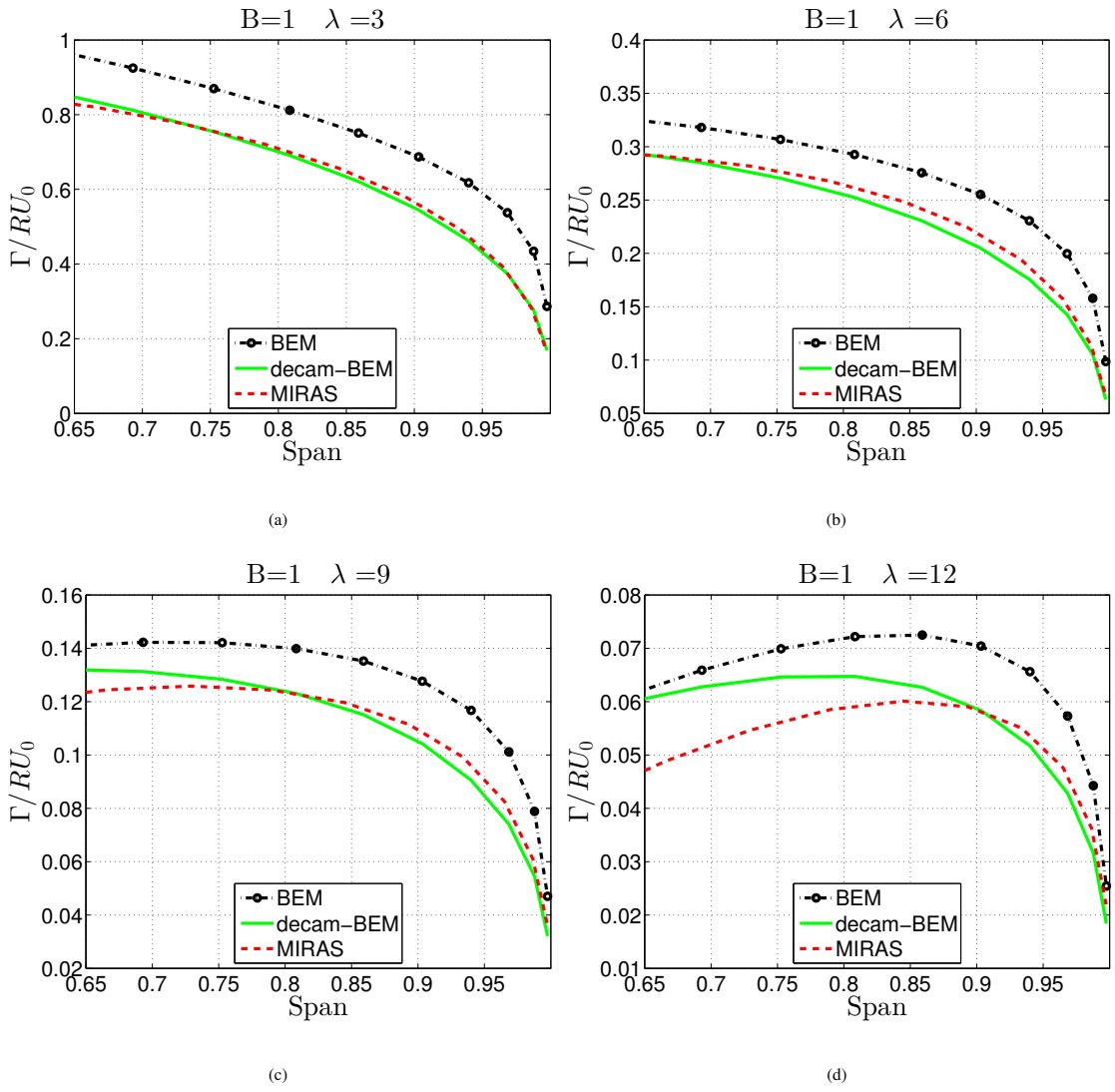

Figure 8. Distributions of normalized circulation, Γ/RU_o, for the single blade optimum rotor . a) λ = 3, b) λ = 6, c) λ = 9, d) λ = 12.

DOI: 10.1002/we

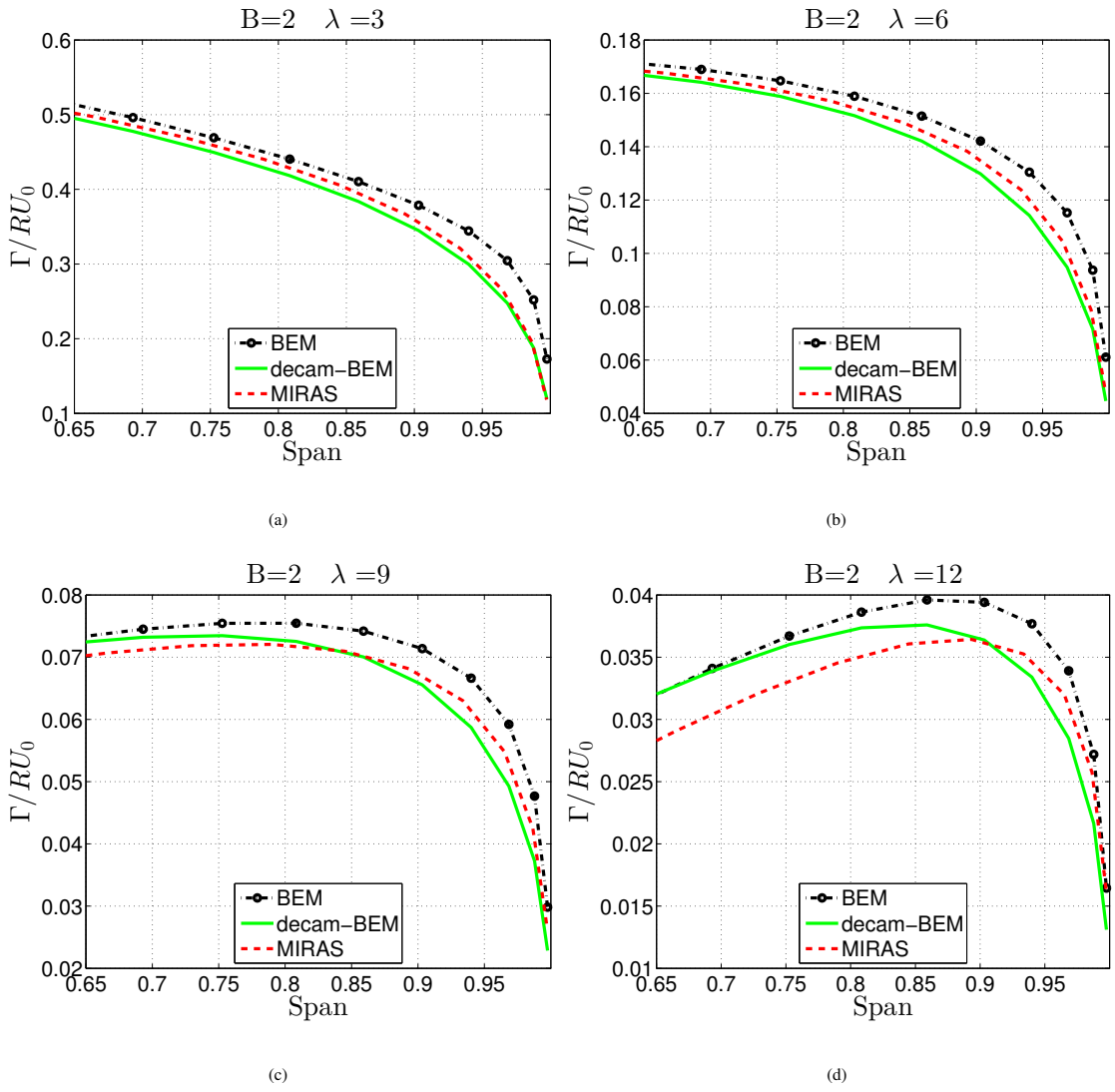

Figure 9. Distributions of normalized circulation, Γ/RU_o, for the two bladed optimum rotor. a) λ = 3, b) λ = 6, c) λ = 9, d) λ = 12.

Wind Energ. 2010; **00**:1–26 © 2010 John Wiley & Sons, Ltd.

DOI: 10.1002/we

Prepared using weauth.cls

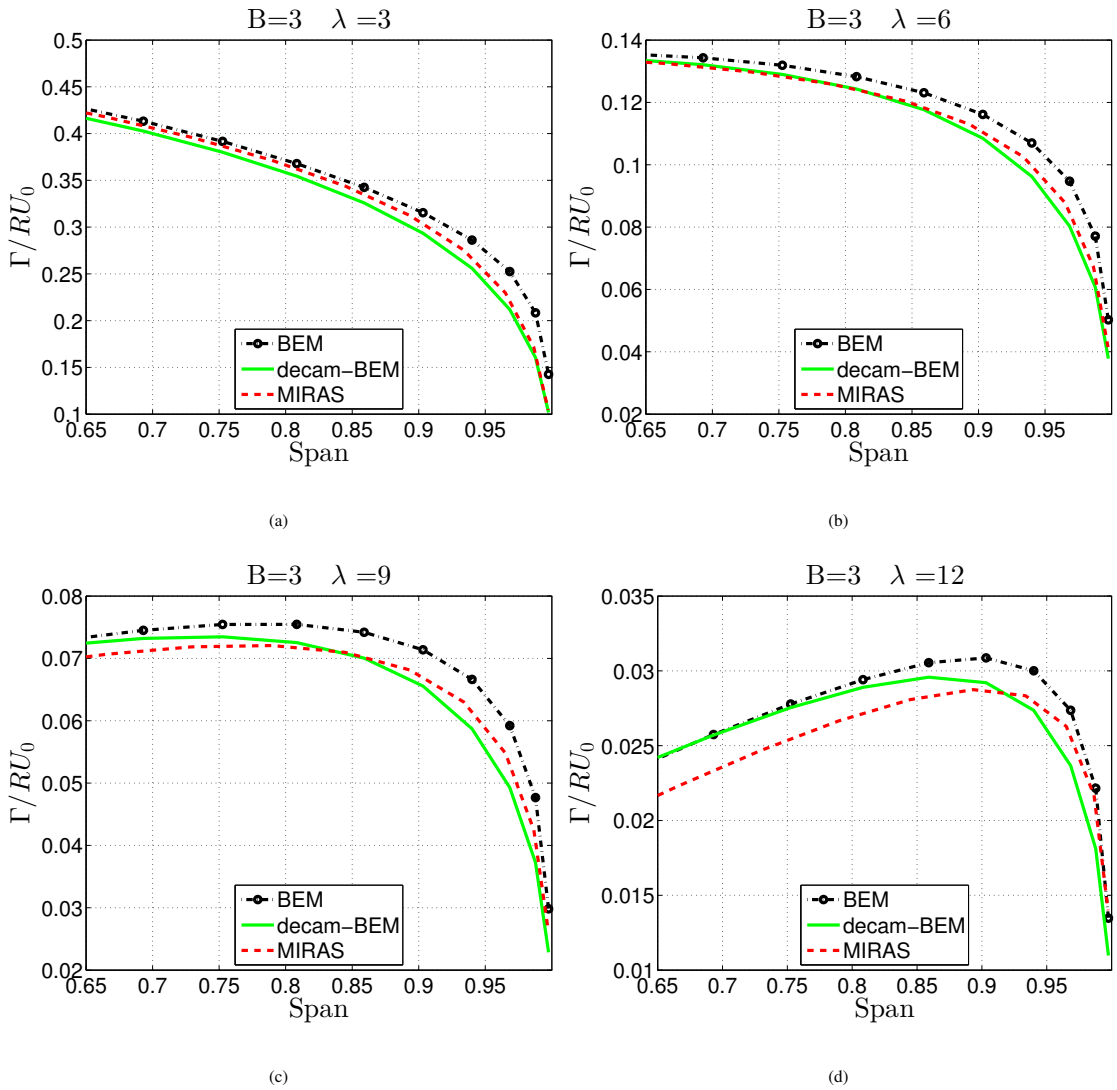

Figure 10. Distributions of normalized circulation, Γ/RU_o, for the three bladed optimum rotor . a) λ = 3, b) λ = 6, c) λ = 9, d) λ = 12.

DOI: 10.1002/we

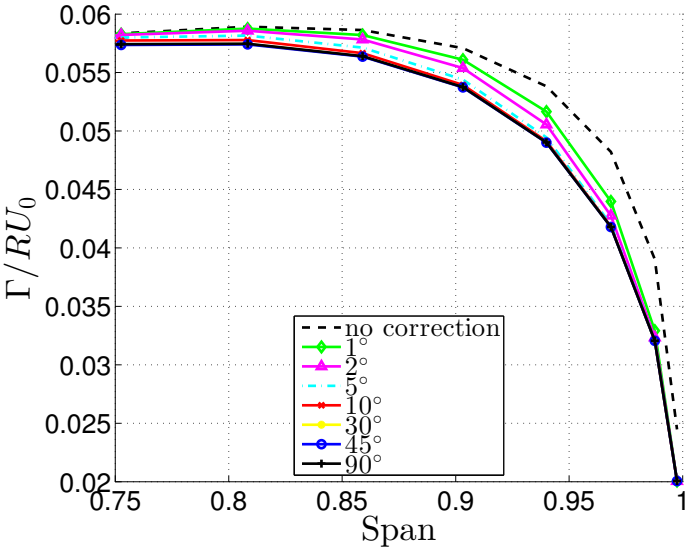

Figure 11. Wake length dependency of the decambering correction.

Wind Energ. 2010; **00**:1–26

DOI: 10.1002/we

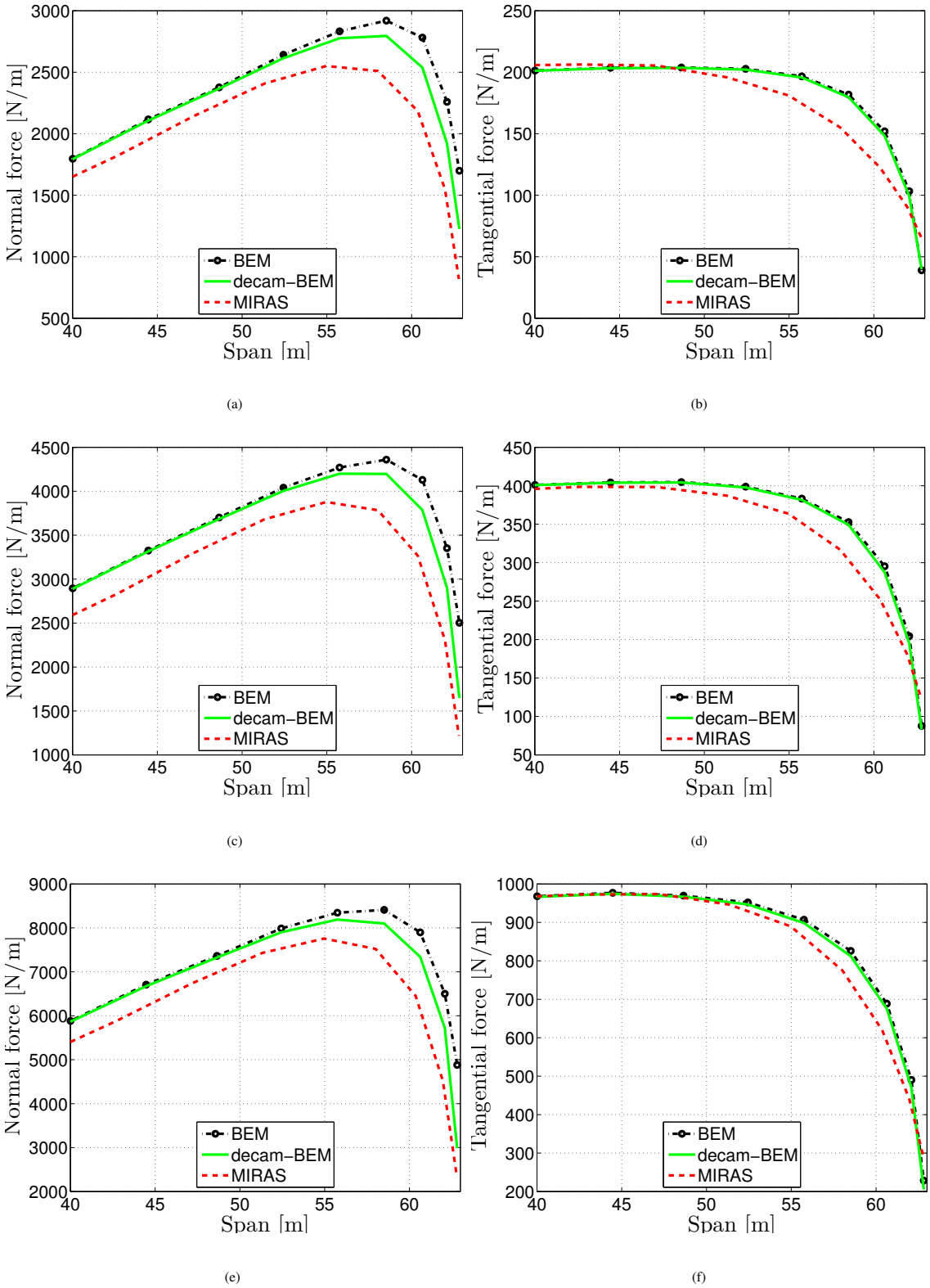

Figure 12. Force distributions for the NREL 5 MW virtual rotor.

a)Normal force, U_0 = 6m/s, b)Tangential force, U_0 = 6m/s, c)Normal force, U_0 = 8m/s,

d)Tangential force, U_0 = 8m/s, e)Normal force, U_0 = 12m/s, f)Tangential force, U_0 = 12m/s

DOI: 10.1002/we

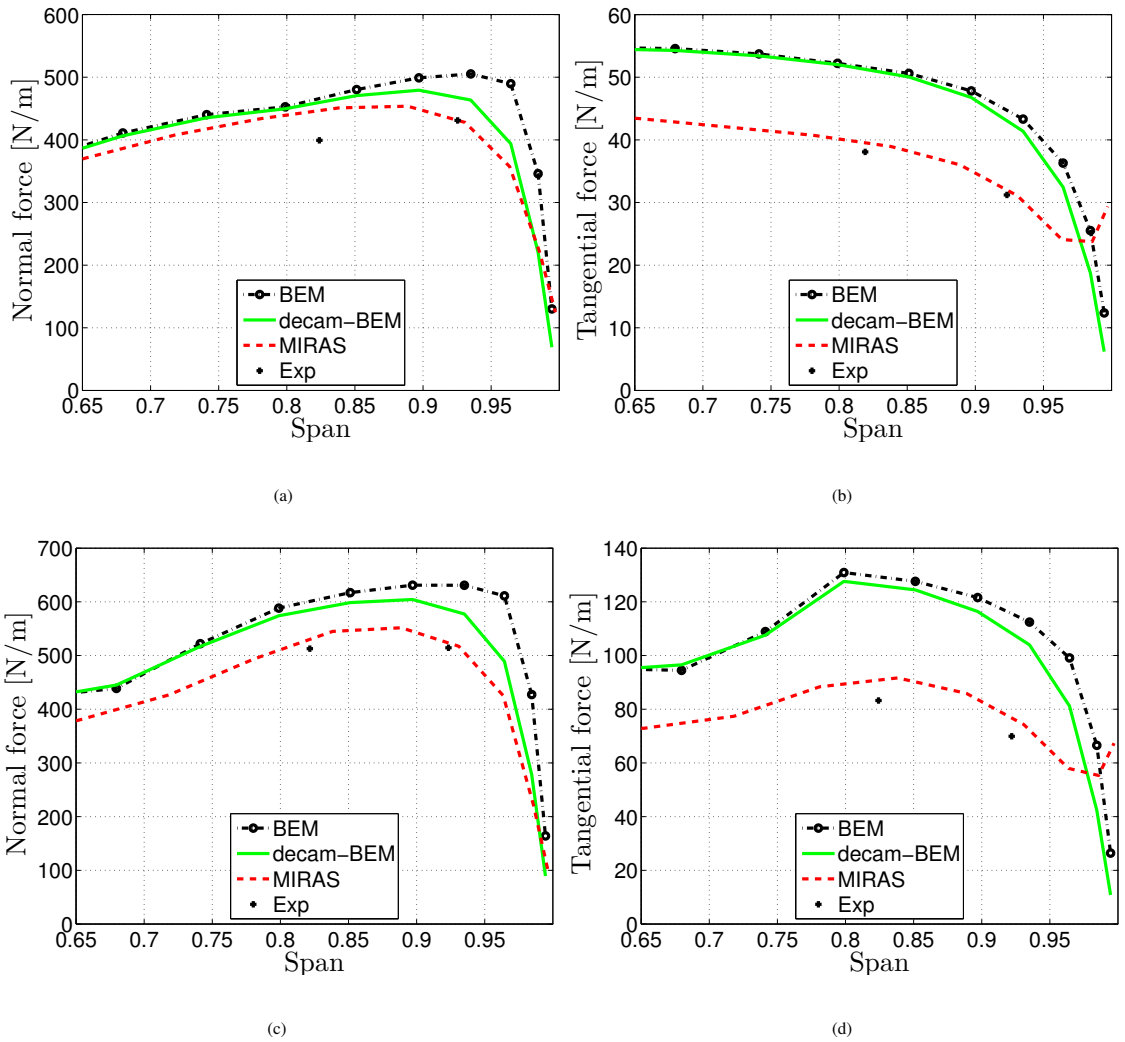

Figure 13. Force distributions for the MEXICO model rotor.

a)Normal force, U_0 = 15m/s, b)Tangential force, U_0 = 15m/s,

c)Normal force, U_0 = 24m/s, d)Tangential force, U_0 = 24m/s

Wind Energ. 2010; **00**:1–26 © 2010 John Wiley & Sons, Ltd.

DOI: 10.1002/we

Prepared using weauth.cls

REFERENCES

1. Betz, A. Schraubenpropeller mit geringstem energieverlust - mit einem zusatz von L. Prandtl. *Göttinger Klassiker der Strömungsmechanik*, 1919; **3**: 68-88.
2. Goldstein, S., On the vortex theory of screw propellers. *Technical report*, St. Johns College, Cambridge, 1929.
3. Tollmien, W., Schlichting, H. and Görtler, H. (1961) *Ludwig Prandtl Gesammelte Abhandlungen zur angewandten Mechanik, Hydro- und Aerodynamik*. Springer-Verlag 1961.
4. Glauert, H., Airplane propellers, division l. *Aerodynamic Theory* 1935; **4**: 169-360.
5. De Vries, O., Fluid Dynamic Aspects of Wind Energy Conversion. *AGARDograph 243*. ISBN 92-835-1326-6, 1979.
6. Shen, W.Z., Mikkelsen, R., Sørensen, J.N. and Bak, C. Tip loss Corrections for Wind Turbine Computations. *Wind Energy* 2005; **8**: 457-475.
7. Sørensen, J.N. and Shen, W.Z. Numerical Modelling of Wind Turbine Wakes. *Journal of Fluids Engineering* 2002; **124**: 393-399.
8. Montgomerie, B. De-camber: Explanation of an effect of lift reduction near the tip caused by the local flow around airplane wings or wind turbine tips. *Proc. Plenary meeting of the group for Dynamic Stall and 3D Effects a European Union, Joule 2 project*. Cranfield Institute of Technology, 1995, April 3-4.
9. Migliore, P.G., Wolfe, W.P. and Fanucci, J.B. Flow Curvature Effects on Darrieus Turbine Blade Aerodynamics. *Journal of Energy* 1980; **4**: 49-55.
10. Bianchini, A., Ferrari, L. and Carnevale, E. A model to account for the virtual camber effect in the performance prediction of an H-Darrieus VAWT using the momentum models. *Wind Engineering* 2011; **35**: 465-482.
11. Mukherjee, R. and Gopalarathnam, A. Poststall prediction of multiple-lifting-surface configurations using a decambering approach. *Journal of Aircraft* 2006; **43**: 660-668. doi:10.2514/1.15149.
12. Katz, J. and Plotkin, A. *Low-speed aerodynamics.* McGraw-Hill, New York, 2001.
13. Hansen, Martin O.L. *Aerodynamics of wind turbines* Earthscan, 2008.
14. Ramos-García, N., Sørensen J.N. and Shen W.Z. A strong viscous-inviscid interaction model for rotating airfoils. *Wind Energy* 2013. 10.1002/we.1677
15. Ramos-García, N., Sørensen J.N. and Shen W.Z. Validation of a three-dimensional viscous-inviscid interactive solver for wind turbine rotors. *Renewable Energy* 2014; **70**: 78-92.
16. Burton, T., Sharpe, D., Jenkins, N. and Bossanyi, E. *Wind Energy Handbook.* John Wiley & Sons, Ltd, New York, 2002.

DOI: 10.1002/we

17. Jonkman, J., Butterfield, S., Musial, W. and Scott, G. Definition of a 5-MW Reference Wind Turbine for Offshore System Development. *Technical Report*, NREL/TP-500-38060, National Renewable Energy Laboratory, Golden, Colorado, USA, 2009.

18. Schepers, J.G. and Snel, H. Model Experiments in Controlled Conditions, *Final Report*, The Energy Research Center of the Netherlands, ECN-E–07-042, 2007.

Wind Energ. 2010; **00**:1–26 © 2010 John Wiley & Sons, Ltd.

DOI: 10.1002/we

Prepared using weauth.cls